



## Characterizing the composition and evolution of and urban particles in Chongqing (China) during summertime



Yang Chen<sup>a,b</sup>, Fumo Yang<sup>a,c,\*</sup>, Tian Mi<sup>a</sup>, Junji Cao<sup>b</sup>, Guangming Shi<sup>a</sup>, Rujin Huang<sup>b,d</sup>, Huanbo Wang<sup>a</sup>, Jun Chen<sup>e</sup>, Shengrong Lou<sup>f</sup>, Qiyuan Wang<sup>b</sup>

<sup>a</sup> Key Laboratory of Reservoir Aquatic Environment of CAS, Chongqing Institute of Green and Intelligent Technology, Chinese Academy of Sciences, Chongqing 400714, China

<sup>b</sup> Key Lab of Aerosol Chemistry & Physics, Institute of Earth Environment, Chinese Academy of Sciences, Xi'an 710061, China

<sup>c</sup> Center for Excellence in Regional Atmospheric Environment, Institute of Urban Environment, Chinese Academy of Sciences, Xiamen 361021, China

<sup>d</sup> Laboratory of Atmospheric Chemistry, Paul Scherrer Institut (PSI), CH-5232 Villigen PSI, Switzerland

<sup>e</sup> School of Energy and Power Engineering, University of Shanghai for Science and Technology, Shanghai 200093, China

<sup>f</sup> Shanghai Academy of Environmental Sciences, Shanghai 200233, China

### ARTICLE INFO

#### Article history:

Received 15 July 2016

Received in revised form 3 December 2016

Accepted 5 December 2016

Available online 7 December 2016

#### Keywords:

Mixing state

Atmospheric process

Single particle

Chongqing

### ABSTRACT

Urban particles were investigated using a single particle aerosol mass spectrometer (SPAMS) in Chongqing during the summertime (from 07/05/2014 to 08/06/2014). Chemical composition, mixing state, and atmospheric behavior of urban particles were studied. The major particle types include ECOC (Elemental-Carbon-Organic-Carbon 20.6%), OC (20.1%), KSec (K-Secondary) (13.3%), BB (Biomass burning, 11.9%), NaK (sodium-potassium-rich, 7.3%), Al-rich (4.0%), Fe-rich (3.2%), Ca-rich (1.4%), Ca-EC (1.6%), and NaKPb (0.5%). EC, ECOC, OC, and Ca-EC were prevalent in the condensation mode ( $<0.7 \mu\text{m}$ ), while KSec, EC, NaK were significant in both the droplet mode (0.7–1.1  $\mu\text{m}$ ) and coarse mode. Increases in aged groups such as EC, KSec, and NaK were observed in the afternoon. Case studies suggested that wet scavenging (rain) rates of different single particle types followed an order of NaKPb > Fe-rich > EC > Ca-EC > Ca-rich > KSec > OC > NaK > ECOC > Al-rich > BB. Increased number fraction of EC and KSec were correlated with the increase of odd oxygen ( $O_x = O_3 + NO_2$ ). EC, OC, and ECOC were enriched at higher relative humidity. The findings of this study on the mixing state, temporal variation, processing, and evolution of single particles provide new insight into the atmospheric behavior and impacts of urban particles.

© 2016 Elsevier B.V. All rights reserved.

### 1. Introduction

Airborne particulate matter (PM) affects visibility, climate, and human health (Pöschl, 2005). PM has a complex chemical composition with various sources, behaviors, and impacts (Zamora et al., 2013). Understanding the size-resolved chemical mixing state of atmospheric PM is essential to predict its health impact and to develop effective and efficient abatement strategies to abate PM (Qin et al., 2012). In addition, size-resolved chemical mixing state information has been used to study the climate-relevant properties of PM, such as hygroscopic growth, ice nucleation, and cloud condensation (CCN) activities (Corbin et al., 2012; Dall'Osto et al., 2004; Formenti et al., 2011; Healy et al., 2014; Herich et al., 2009; Murphy et al., 2006; Su et al., 2010).

Aerosol time-of-flight mass spectrometer (ATOFMS) is a valuable tool for investigating the size-resolved chemical composition of ambient PM, and is capable of identifying organic carbon (OC), elemental carbon (EC), trace metals, and ionic species with high temporal resolution

(Gard et al., 1997). ATOFMS has been widely used worldwide to characterize airborne particle types, mixing state, and sources (Pratt and Prather, 2012). For example, Silva et al. (2000) studied the single particle chemical composition of soil dust from Southern California. Qin and Prather (2006) reported size and chemical composition of individual particles from December 2000 to February 2001, and seasonal variations in Riverside, CA (Qin et al., 2012). In Europe, urban single particle types have been studied in Athens (Dall'osto and Harrison, 2006), London (Dall'Osto and Harrison, 2011), Cork (Dall'Osto et al., 2013a; Healy et al., 2009, 2010), Paris (Healy et al., 2012), and Barcelona (Dall'Osto et al., 2013b). More recently, investigations of single particle types in Chinese cities such as Beijing (Ma et al., 2016), Shanghai (Li et al., 2011; Yang et al., 2010, 2012), Guangzhou (Bi et al., 2011; Ye et al., 2016), Nanjing (H. Wang et al., 2015), and Xi'an (Chen et al., 2016) have been reported, contributing to the understanding of mixing state, chemical composition, and sources at high PM<sub>2.5</sub> concentration levels (Cao, 2014). Particle types in these cities were mainly carbonaceous particles and dust (Chen et al., 2016). Despite the above studies, there are other areas in China that experience severe particulate pollution but whose particle composition is poorly understood.

\* Corresponding author.

E-mail address: [fmyang@cigit.ac.cn](mailto:fmyang@cigit.ac.cn) (F. Yang).

Chongqing is an inland, subtropical, and industrial city on the edge of the Sichuan Basin, Southwestern China, with a population of 8.23 million (National-Statistics, 2014). Summer in Chongqing is long and among the most humid in China. Local economy has expanded rapidly in recently years, and the particulate pollution has drawn attentions more recently, but the knowledge of local PM chemical composition, sources, evolution, and impacts is still limited (Ye et al., 2007).

This study aims to characterize the size-resolved chemical composition, mixing state, and the atmospheric processing of PM using a Single Particle Aerosol Mass Spectrometer (SPAMS) in urban areas of Chongqing during the summertime of 2014. The investigation of urban single particles under high temperature and humidity conditions is helpful for understanding the atmospheric behavior and impacts of different single particle types in the context of particulate pollution in China.

## 2. Methodology

### 2.1. Field measurement

A SPAMS was deployed in an urban background air quality supersite from 07/05/2014 to 08/06/2014. The supersite is located on the roof of a commercial office building (106.51°E, 29.62°N), with a height of 30 m above the ground, surrounded by business and residential communities. No industry exists within 20 km around the sampling site. Meteorological, trace gasses, and PM measurements were also conducted on site.

### 2.2. Instrumentation

SPAMS has been described in the literature (Li et al., 2011). Briefly, single particles with a size range of 0.1–3.0  $\mu\text{m}$  are focused into a narrow beam through an aerodynamic lens and arrive at the sizing region. In the sizing region, two separated, diode-pumped Nd:YAG lasers ( $\lambda = 532 \text{ nm}$ ) are used to determine the vacuum aerodynamic diameter by measuring the time-of-flight of passing particles. Then a Nd:YAG laser (266 nm,  $\sim 1 \text{ mJ/pulse}$ ,  $1 \times 10^8 \text{ W/cm}^2$ , UL728F11-F115, Quantel, France) is used to desorb and ionize particles arriving at the mass spectrometer. The resulting positive and negative ions enter the flight tubes of the mass spectrometer and generate bipolar ion mass spectra.

During sampling, a diffusion drier was connected to the SPAMS to remove aerosol water. The hit rate variations before, during, and after raining was also extracted, and it changed with a range of 0–2%.  $\text{PM}_{2.5}$  mass was measured using a Tapered Element Oscillating Microbalance (TEOM 1400a) with a time resolution of 1 min. Temperature, wind direction, wind speed, and relative humidity (RH) were monitored from an automatic meteorological station (Vaisala MAWS201). Ambient  $\text{NO}_x$  ( $\text{NO}$ ,  $\text{NO}_2$ ) were monitored using a chemiluminescence nitrogen oxides analyzer (Thermo 42i).  $\text{SO}_2$  and  $\text{O}_3$  were monitored using  $\text{SO}_2$  (Thermo 43) and  $\text{O}_3$  monitors (Thermo 49), respectively.

### 2.3. Data analysis

A total of 456,068 particles were collected with validated mass spectra (30 units above the baseline) and a hit rate range of 12–25%. The SPAMS dataset was imported into YAADA (Yet Another Data Analyzer Toolkit), with which single particle types were grouped. The parameter setting for this analysis was: learning rate 0.05, vigilance factor 0.80, and iterations 20. The ART-2a clustering procedure generated 278 clusters, and then these clusters were manually merged based on similar ion mass spectra pattern, temporal trend, and size distribution (Dall'osto and Harrison, 2006). The clusters used to describe the total SPAMS dataset was then reduced to 11, with an unidentified group named as Other.

## 3. Results and discussion

### 3.1. Overview

The measurements period was 07/05/2014 (mm/dd/yyyy) to 08/06/2014. The temporal trends of temperature, RH, trace gasses,  $\text{PM}_{2.5}$ , and  $\text{PM}_{1.0}$  are shown in Fig. 1. The average temperature was  $30 \pm 5 \text{ }^\circ\text{C}$ ; RH was  $60 \pm 17\%$ . The wind was mainly from the north, northeast, and northwest (Fig. S1), with a wind speed of  $1.6 \pm 0.7 \text{ m s}^{-1}$ . The ratio of  $\text{PM}_{1.0}/\text{PM}_{2.5}$  was  $0.70 \pm 0.31$ ; submicron particles were important during summertime.

### 3.2. SPAMS particle type characterization

The average mass spectra of revolved particle types are shown in Fig. 2. Ions such as carbon cluster ( $\text{C}_n^+/\text{C}_n^-$ , mass to charge ratio,  $m/z \pm 12, \pm 24, \pm 36\dots$ ), potassium ( $m/z$  39 and 41), sodium ( $m/z$  23), sulfate ( $m/z$  –97 and –80), and nitrate ( $m/z$  –46 and –62) were commonly found in all particle types. The summary of single particle types with their number fractions and chemical composition is listed in Table 1.

**BB.** The mass spectra were composed of sodium ( $m/z$  23), carbon ion fragments, potassium,  $\text{CN}^-$ ,  $\text{CNO}^-$ , and the presence of  $m/z$  –45, –59, and –71. These marker ions are indicative of biomass burning particles (Healy et al., 2010; Silva et al., 1999). The absence of  $\text{K}_2\text{Cl}$  also suggests the BB type had aged after leaving the emission plume (Silva et al., 1999).

**KSec.** As a kind of aged BB particle type, it contained  $\text{K}^+$ ,  $\text{Al}^+$ ,  $\text{CN}^-$ ,  $\text{CNO}^-$ , sulfate, nitrate,  $\text{SiO}_3^-$  ( $m/z$  –76),  $\text{SiO}_2^-$  ( $m/z$  –60), and  $\text{PO}_3^-$  ( $m/z$  –79). KSec was rich in  $\text{SiO}_3^-$ , which is commonly from soil particles. Based on the uptake of sulfate and nitrate and its size distribution, KSec was more aged than the BB particle type.

**Nak.** NaK was strongly associated with sodium and potassium. The negative spectrum contained carbon ion clusters,  $\text{CN}^-$ ,  $\text{CNO}^-$ , nitrate, sulfate,  $\text{SiO}_3^-$ , and phosphate. NaK was similar to the NaEC particle type reported by Moffet et al. (2008) that was emitted from industrial emissions/incineration/refuse burning.

**Fe-rich.** Fe-rich particles contained a strong iron signal ( $m/z$  56 and 54), as well as potassium, and sodium. The absence of a strong  $\text{Ca}^+$  signal ( $m/z$  40) indicates that the  $m/z$  56 peak was not  $\text{CaO}^+$ . Nitrate, sulfate, and phosphate were present in the negative spectrum. The present of BB markers like  $\text{CN}^-$ ,  $\text{CNO}^-$ , and chloride ( $m/z$  –35 and –37) suggested the contribution of BB particles (Sullivan et al., 2007). Fe-rich pointed to soil dust particles from building yards and unpaved roads that are common in some Chinese cities (Huang et al., 2014).

**Ca-rich.** This particle type was characterized with strong calcium and potassium peaks in the positive mass spectra. The  $m/z$  56 signal was a mixture of  $\text{CaO}^+$  and  $\text{Fe}^+$  because of the present of  $m/z$  54 ( $\text{Fe}^+$ ). In the negative spectrum, weak BB ion markers as described above were also found.

**Al-rich.**  $\text{Al}^+$  ( $m/z$  27),  $\text{AlO}^+$  ( $m/z$  43), and  $\text{Al}_2\text{O}^+$  ( $m/z$  70) were found in the positive spectrum. There are also  $\text{K}^+/\text{C}_3\text{H}_3^+$  peaks at  $m/z$  39 and associated OC ion fragments such as  $m/z$  51, 63, and 77. These have previously been attributed to light-duty vehicle emissions (Sodeman et al., 2005) and the combination of these peaks suggests that Al-rich particles are associated with traffic-related road dust (Shen et al., 2016).

**NaKpb.** This type was characterized by a strong lead signal ( $m/z$  206, 207, and 208), and associated peaks from  $\text{K}^+$ ,  $\text{Na}^+$ ,  $\text{Cl}^-$ ,  $\text{CN}^-$ ,  $\text{CNO}^-$ , sulfate, and nitrate. In China, coal burning is an important source of particulate lead (Xu et al., 2012).

**CaEC.** The CaEC type contained carbon clusters, potassium, calcium ( $\text{Ca}^+$ ,  $m/z$  40;  $m/z$  57,  $\text{CaOH}^+$ ),  $\text{C}_2\text{H}_2^-$  ( $m/z$  –26), nitrate, phosphate ( $m/z$  –79), and a minor amount of sulfate. The signal of  $m/z$  –26 was observed, but  $m/z$  –42 ( $\text{CNO}^-$ ) was not found. We therefore assigned  $m/z$  –26 to  $\text{C}_2\text{H}_2^-$  instead of  $\text{CN}^-$  (Dall'Osto et al., 2013a). This cluster contained heavy-duty vehicle emission markers like phosphate and

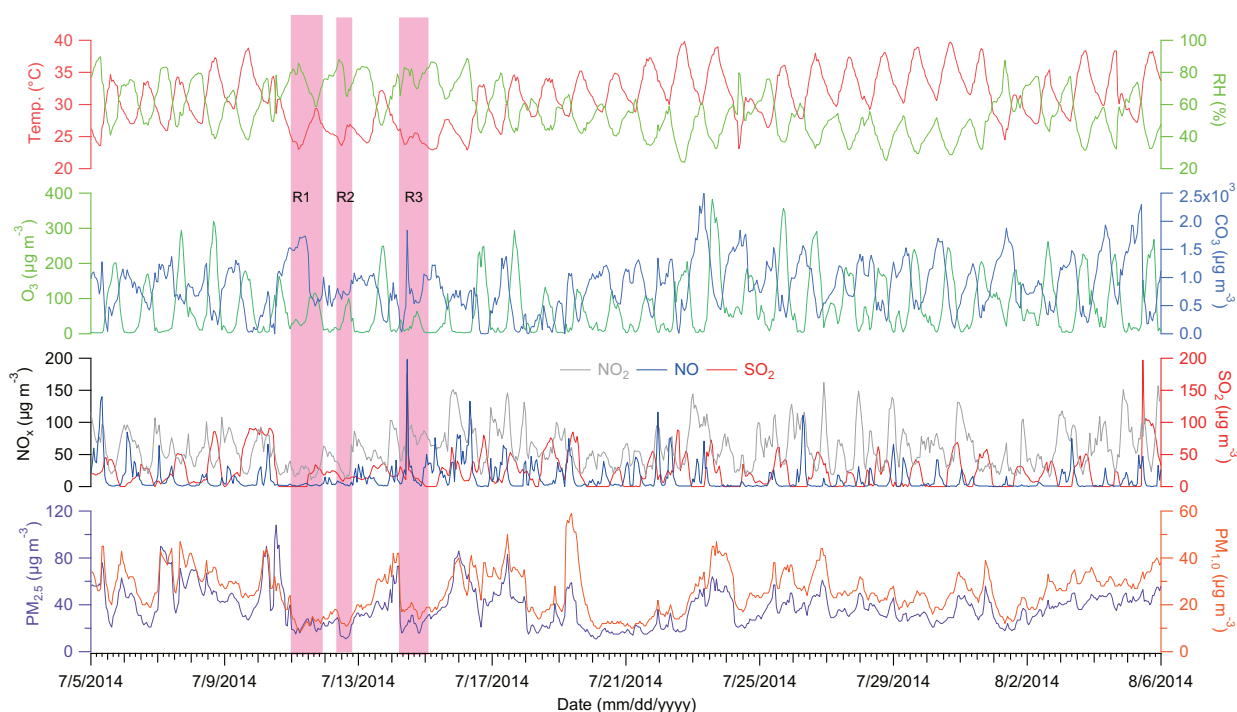


**Fig. 1.** Temporal trends of temperature, relative humidity, gaseous pollutants ( $\text{O}_3$ ,  $\text{CO}$ ,  $\text{NO}$ ,  $\text{NO}_2$ ,  $\text{SO}_2$ ),  $\text{PM}_{2.5}$ ,  $\text{PM}_{1.0}$  in 1 h time resolution. The three pink periods indicate three rain events (R1, R2, and R3).

calcium, which arise from the combustion of lubricating oil (Spencer and Prather, 2006).

**EC.** The EC mass spectra contained carbon clusters,  $\text{K}^+$  ( $m/z$  39), sulfate, and nitrate from traffic exhaust (Healy et al., 2012).

**OC.** The OC particle type was characterized by abundant organic ion fragments, including  $\text{C}_2\text{H}_3^+$  ( $m/z$  27),  $\text{C}_2\text{H}_5^+$  ( $m/z$  29),  $\text{C}_3\text{H}^+$  ( $m/z$  37),  $\text{C}_3\text{H}_3^+$  ( $m/z$  39),  $\text{C}_2\text{H}_3\text{O}^+$  ( $m/z$  43), and monoaromatic hydrocarbon peaks like 51, 63, 77, and 91 in the positive mass spectrum.  $\text{C}_2\text{H}^-$  ( $m/z$  25),  $\text{C}_2\text{H}_2^-$  ( $m/z$  26), and  $\text{C}_4\text{H}^-$  ( $m/z$  -49) were abundant in the negative spectrum. Organic acid marker  $\text{C}_2\text{H}_5\text{COO}^-/\text{C}_2\text{HO}_3^-$  ( $m/z$  -73) was also observed (Zauscher et al., 2013).

**ECOC.** Carbon ions and their adjacent hydrocarbon ion fragments were significantly pronounced in ECOC. For example,  $\text{C}_5^+$  ( $m/z$  60) was associated with  $\text{C}_x\text{H}_y^+$  fragments like  $m/z$  61, 62, 63, and 64. This cluster is usually from an incomplete combustion process (Moffet and Prather, 2009).

Fig. 3 shows the unscaled size distribution of single particle types with a size bin of  $0.1 \mu\text{m}$ . KSec had a fraction of 0.17 for particles with a diameter larger than  $0.70 \mu\text{m}$ . EC was the most abundant cluster in the droplet mode ( $<0.7 \mu\text{m}$ ). The fraction of ECOC was over 0.15 in the size range from  $0.3$  to  $1 \mu\text{m}$ . The fraction of BB had a ratio between 0.08 and 0.12 in all size bins, with an average of 0.11.

The mixing state is defined by the fraction of particles containing a special ion in each particle type. The criteria for selecting ions was referenced and adopted from Moffet et al. (2008). As shown in Fig. 4, over 97% of OC, ECOC, and Ca-rich were found internally mixed with sulfate; over 90% of each single particle type had detectable nitrate. 35% of EC particles contained ammonium, which was higher than in other particle types. The ammonium-rich EC was likely from heavy-duty diesel trucks that were installed with selective catalytic reduction devices to reduce  $\text{NO}_x$  emissions (G. Wang et al., 2015). These devices emit ammonium during operation. Oxalate could be primarily emitted from biomass burning activities (Falkovich et al., 2005), and also secondarily formed via aqueous reactions (Ervens et al., 2011). In our results, 7% and 9% of BB and NaKPb contained oxalate, respectively. Yang et al. (2009) also reported oxalate was internally mixed with ambient biomass burning particles in Shanghai

(China). In our result, 12% of Fe-rich particles contained oxalate. The enrichment of oxalate was also found in mineral dust particles that were rich in iron (Sullivan et al., 2007).  $\text{C}_2\text{H}_3\text{O}^+$  commonly is used as a marker for aldehydes, ketones fragments in SOA (Ng et al., 2011; Zhang et al., 2011), which are produced from photooxidation of their gas phase precursors such as volatile organic compounds (VOCs) and intermediate VOCs (Hallquist et al., 2009).  $\text{C}_2\text{H}_3\text{O}^+$  ( $m/z$  43) significantly distributed in all particle types, especially in OC (0.92) as an ion fragment marker of SOA (Qin and Prather, 2006; Zhang et al., 2011).

### 3.3. Temporal trend and average diurnal pattern analysis

Time series of SPAMS count with a time resolution of 1 h are shown in Fig. S2. The time trend of BB was strongly correlated with OC ( $R = 0.81$ ), NaK ( $R = 0.63$ ), Ca-rich ( $R = 0.65$ ), and ECOC ( $R = 0.58$ ). OC was also correlated with Al-rich ( $R = 0.68$ ), which was a kind of fly ash from soil dust (Silva et al., 2000). The correlations suggest Ca-rich particles were strongly associated with biomass burning. Fe-rich, as a typical road dust particle type (Dall'osto and Harrison, 2006), was well correlated with EC ( $R = 0.77$ ), suggesting EC was mainly from traffic emissions (see below). Additionally, Fe-rich could also be from fly-ash (Li et al., 2012). As expected, it had a good correlation with NaK ( $R = 0.58$ ). The latter was a particle type from incineration or coal burning (Healy et al., 2010). KSec was strongly correlated with NaK ( $R = 0.72$ ), BB ( $R = 0.67$ ), and OC ( $R = 0.57$ ).

As shown in Fig. 5, for the number fraction of particle types, there were no significant differences between weekdays and the weekend except for EC. In weekdays, the number fraction of EC was 1.5 times higher than on weekends, suggesting a higher contribution from traffic on weekdays. However, we could not identify particle types from specific industrial sources because the local industries kept working on weekends.

The average diurnal patterns of RH, temperature, gasses, and number fraction of major SPAMS particle types are shown in Fig. 6. CO and NO showed a sharp morning peak (08:00) due to traffic emissions (Seinfeld and Pandis, 2006).  $\text{O}_3$  had a strong peak in the afternoon

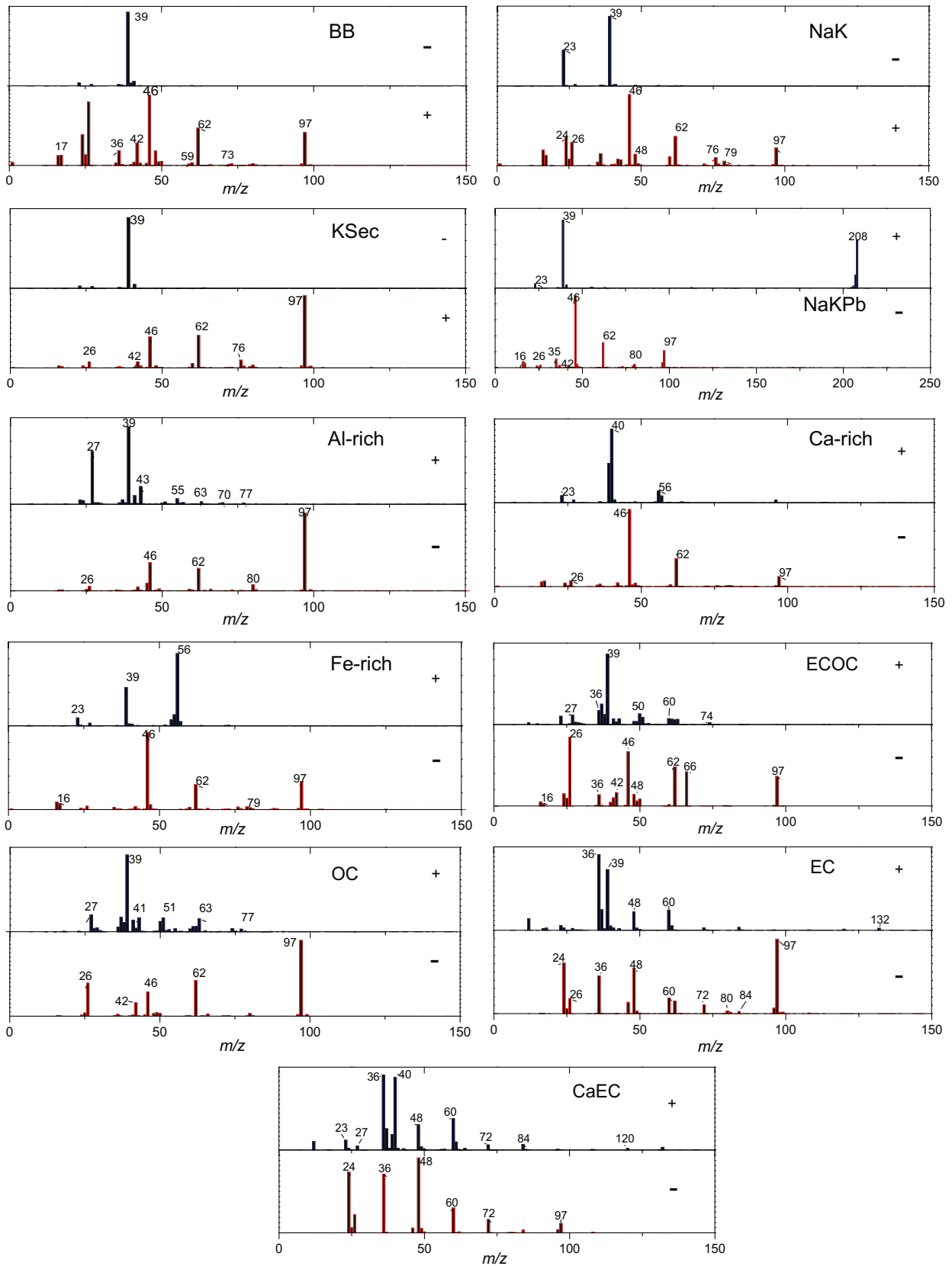


Fig. 2. Average mass spectra for single particle types in Chongqing summer SPAMS dataset, the label in each panel indicates the single particle type.

(16:00), associated with NO depletion. PM<sub>2.5</sub> showed the evening (0:00 a.m.) and early morning (5:00 a.m.) peaks. The evening peak occurred due to the suppression of the planetary boundary layer; a possible

reason for the latter effect will be discussed below. PM<sub>1.0</sub> concentration decreased with rising temperature and had a morning peak starting at 8:00 a.m. due to the morning rush hour.

**Table 1**

Summary of single particle types, number counts, percentage, typical chemical ions, and possible sources in the Chongqing SPAMS dataset during summer 2014.

Cluster	Count	%	Chemical composition	Possible sources
ECOC	68,256	20.6	$K^+$ , $C^\pm$ , OC ( $C_xH_y^+$ , $C_xH_yO_z^+$ ), $SO_4^-$ , and $NO_3^-$	Traffic
OC	66,419	20.1	$C_2H_2^+$ , $C_4H_3^+$ , $C_3H^+$ , $C_3H_3^+$ , $C_2H_3O^+$ , $C_4H_3^+$	Traffic
EC	49,088	14.8	$K^+$ , $C^\pm$ , $SO_4^-$ , and $NO_3^-$	Traffic
KSec	44,114	13.3	$CN^-$ , $CNO^-$ , $SO_4^-$ , $NO_3^-$ , $SiO_3^-$ , and $PO_3^-$	Secondary
BB	39,247	11.9	$K^+$ , $CN^-$ , $CNO^-$ , $SO_4^-$ , $Cl^-$ , and $NO_3^-$	BB
NaK	24,142	7.3	$CN^-$ , $CNO^-$ , $NO_3^-$ , $SO_4^-$ , and $PO_3^-$	BB, Coal
Al-rich	13,067	4.0	$Al^+$ , $AlO^+$ , $Al_2O^+$ , OC, $CN^-$ , $CNO^-$ , $SO_4^-$ , and $NO_3^-$	Road dust
Fe-rich	10,715	3.2	Fe, $PO_3^-$ , OC, $NO_3^-$ , and $SO_4^-$	Soil, dust
Ca-rich	4685	1.4	$K^+$ , $Ca^+$ , $CaO^+$ , $SO_4^-$ , and $NO_3^-$	Soil, dust
Other	3877	1.2	–	Unknown
CaEC	5402	1.6	$Ca^+$ , $C^\pm$ , $C_2H_2^+$ , $NO_3^-$ , and $PO_3^-$	Traffic
NaKPb	1742	0.5	$Pb^+$ , $K^+$ , $Na^+$ , $Cl^-$ , $CN^-$ , $CNO^-$ , $SO_4^-$ , and $NO_3^-$	Combustion

As shown in Fig. 6e, EC started increasing at 7:00, reached the first peak around 9:00, and peaked again around 16:00. As typical pollutants from traffic emissions, NO and EC would normally have a strong correlation in their diurnal profiles (Seinfeld and Pandis, 2006). However, in our study, the diurnal pattern of EC was clearly not strongly coupled with NO. NO was rapidly depleted by the increase of ozone (Seinfeld and Pandis, 2006). OC had morning (8:00) and evening (20:00) peaks and was at a minimum in the afternoon. The OC diurnal profile was consistent with the diurnal profiles of primary organic aerosol in aerosol mass spectrometer studies (Zhang et al., 2011). The diurnal pattern of ECOC was consistent with the behavior of ECOC that was reported in Xi'an during wintertime (Chen et al., 2016). NaK and KSec had afternoon peaks at 16:00 when ozone reached its highest concentrations, suggesting the existence of strong inverse correlations between ozone and these two aged groups (NaK and KSec, respectively). BB did not show a clear diurnal trend, indicating it was a “background” particle type that was transported to the urban area from the countryside. Ca-rich particles were surrogates of biomass burning fly ash (see Section 3.2) and also had an irregular diurnal profile. Fe-rich particles, pointing to a surrogate of soil dust particles, occurred with an early morning peak (4:00–6:00) and daytime peaks (12:00 and 16:00). The daytime peak of the Fe-rich type could be associated with building activities and resuspension from unpaved road. However,

according to the local traffic regulations, heavy-duty trucks were only allowed to enter the urban area between 0:00–5:00. Thus heavy-duty truck emissions possibly caused the morning peaks of Fe-rich, OC, EC, and ECOC, and  $PM_{2.5}$ .

### 3.4. Wet scavenging of PM: a case study

There were three rain events during the observation period, which occurred on 07/11 (R1, 0:00 to 6:00, 6 h), 07/12 (R2, 8:00 to 23:00, 15 h), and 07/14 (R3 from 4:00 to 17:00, 13 h). These events provide insight into the wet scavenging properties of different particle types. In these episodes, hourly precipitation was between 0.1 and 0.8 mm, with an average of 0.5 mm. Both  $PM_{2.5}$  and  $PM_{1.0}$  decreased dramatically by 30%–50% after one h rain. The average  $PM_{1.0}/PM_{2.5}$  ratio was 0.60, 0.8, and 0.6 again before, in, and after rainfall (Fig. 1). Compared to  $PM_{1.0}$ , the supermicron PM was more easily removed by rain. The average removal ratio of each single particle cluster, calculated as the percent of hourly SPAMS number count, is summarized in Table 2. The mean wet scavenging rate of all single particle types was ~0.50 per hour. NaKPb particle had a wet scavenging rate of  $0.67 \pm 0.24$ , followed by Fe-rich ( $0.60 \pm 0.12$ ), and EC ( $0.58 \pm 0.09$ ). However, the scavenging rate of BB was  $0.26 \pm 0.12$ , similar to ECOC ( $0.26 \pm 0.12$ ), and Al-rich ( $0.31 \pm 0.22$ ). NaKPb and Fe-rich were mainly present with larger mean diameters (0.7  $\mu$ m or higher), while BB, ECOC, and Al-rich peaked around 0.5  $\mu$ m in the unscaled size distribution. Qualitatively, the particle scavenging rate is determined by the size distribution of raindrop and particle. The summer raindrop is supposed to be large in size, which decreases the wet scavenging rate (Seinfeld and Pandis, 2006). However, it also should be noted that, without the data from a particle sizer, we were not able to scale the SPAMS count dataset to the actual number concentration of ambient particles, thus this case study is semi-quantitative. As an aged type with significant uptake of sulfate and nitrate, EC had a faster scavenging rate than BB. It seems that the solubility and hydrophilicity of particles also affects particle wet scavenging rate.

During raining, all hourly particle type counts remained at a low level (usually lower than 50 count  $h^{-1}$ ), except EC and ECOC. Although aged EC and ECOC tended to be removed by rain because they tend to be more hydrophilic (Chen et al., 2014), freshly-emitted EC and ECOC are hydrophobic and do not easily coagulate with or dissolve in a raindrop (Seinfeld and Pandis, 2006).

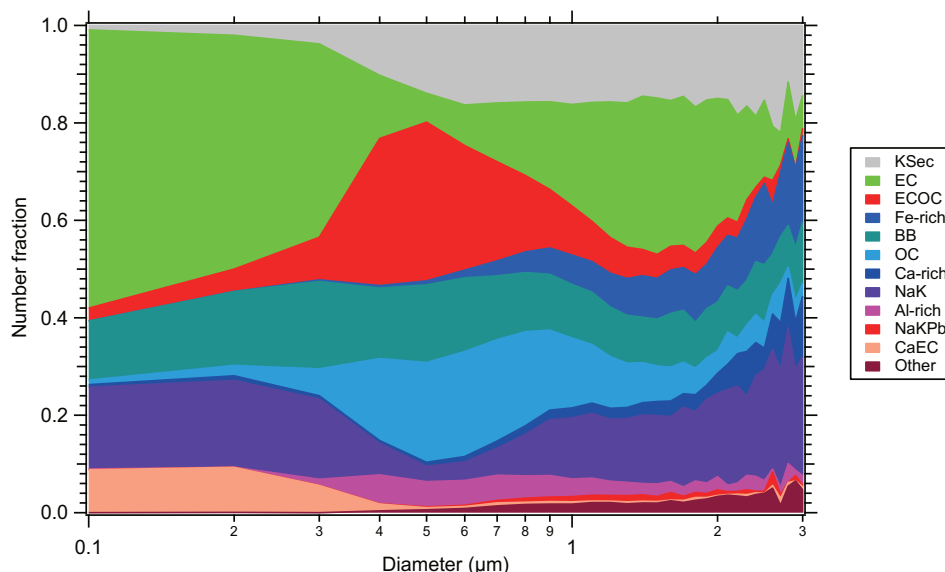


Fig. 3. Unscaled size-resolved number fraction of single particle types in a size bin of 0.1  $\mu$ m during the observation.

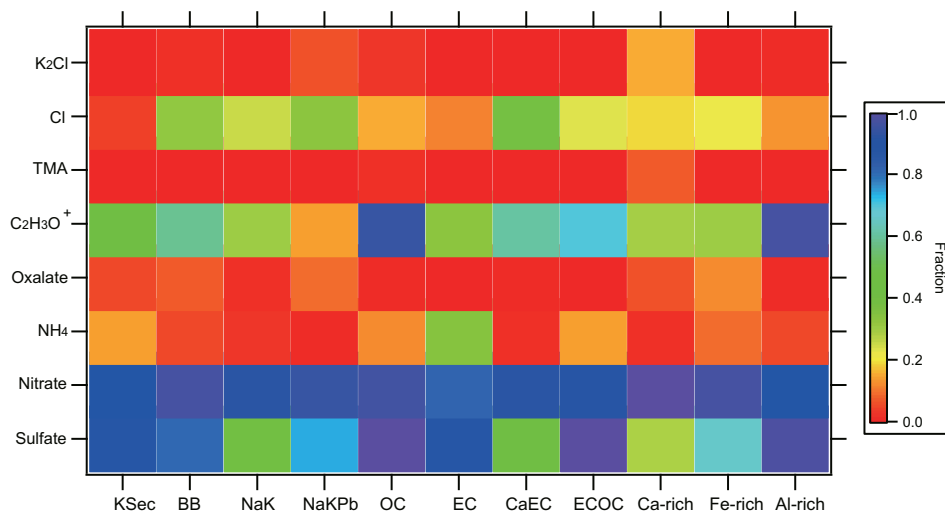


Fig. 4. Number fraction of selected ion markers associated with single particle types represented by the color scale.

### 3.5. Effects of $O_x$ ( $NO_2 + O_3$ ) on the evolution of single particle types

Atmospheric aging processes of aerosols include secondary aerosol formation via pathways such as gas/particle phase partitioning, surface and aerosol phase reactions. These processes produce shifts in morphology, chemical composition, and mixing state (Cubison et al., 2011; Donahue et al., 2012; Hallquist et al., 2009; Kroll et al., 2012; Pratt et al., 2011). The timescale for mixing of semivolatile compounds into particles is several hours, which is relevant to atmospheric transport and diurnal cycling (Ye et al., 2016).

We use odd oxygen concentration ( $O_x = O_3 + NO_2$ ) to represent oxidation level (Zamora et al., 2013) to investigate its effects on single particle types. As shown in Fig. 7a, KSec and EC demonstrated increasing trends against  $O_x$ . To examine the validation of reclassification between different particle types, we extracted the unscaled daily average size distribution of particle types when  $O_x < 100$  ppb and when  $O_x > 100$  ppb (Fig. 8). Only ECOC and KSec had noticeably different size distributions under different atmospheric oxidative conditions. It should be noted that the size distribution of ECOC was not significantly different and was still within the size range of efficient collection of the aerodynamic lens equipped on SPAMS. We are thus confident that the different trends were not caused by instrumental collection bias. The fraction of EC increased by 1.8 times when the  $O_x$  concentration increased from 60 ppb to 140 ppb. As expected, primary particle types like BB, OC,

CaEC, and OCEC were suppressed due to the removal of semi-volatile species in particle phase (Robinson et al., 2007). When  $O_x$  was higher than 160 ppb, the enhancement of ECOC and OC suggests some mixing of SOA on these particle types from photochemical activities. This result implies that odd oxygen influenced not only PM mass (Elser et al., 2016; Sun et al., 2013) but also the number fractions of single particles. In a previous study, we reported a unique case of stagnant meteorological conditions with an average wind speed of  $0.2 \text{ ms}^{-1}$  that minimized dispersion and long-range transport of PM. Under these conditions, reclassification among particle types was observed (Chen et al., 2016). Moffet and Prather (2009) reported the difference between fresh and aged soot as a case of reclassification between particle types. In a thermal desorption study of urban particles in Shanghai, the removal of volatile and semi-volatile species caused significant changes in the biomass burning particle mass spectra, resulting in an aged BB particle type (Zhai et al., 2015). The same effect of reclassification should occur among particle types in the atmosphere.

We also extracted the mean peak area information of secondary species like sulfate, nitrate, oxalate, and  $C_2H_3O^+$  in the variation of  $O_x$ . Although the peak area only semi-quantitatively represents mass concentration and has large uncertainties in single particle studies (Gross et al., 2000; Healy et al., 2014), it is still able to reveal trends in secondary species. As shown in Fig. 7e, the peak area of sulfate and nitrate increased as a function of  $O_x$ , especially when  $O_x$  was over 100 ppb. As

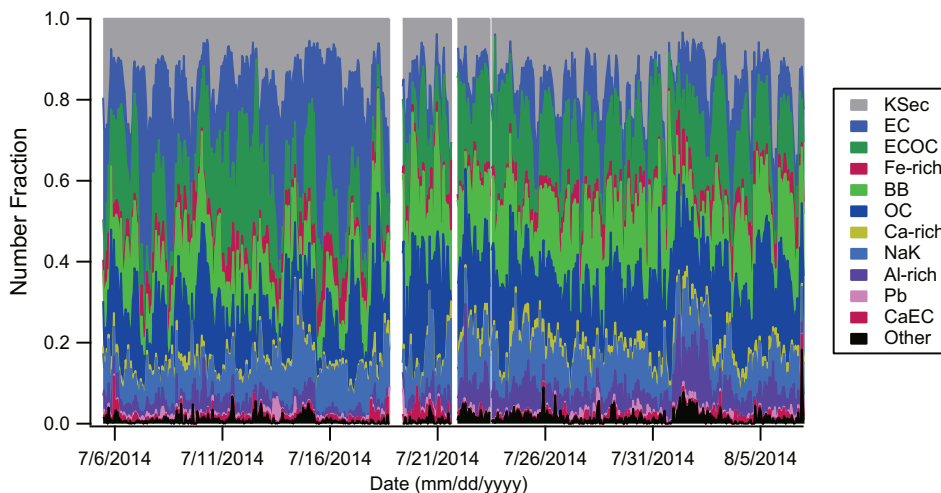


Fig. 5. Time trends of the number fraction of single particle types during observation.

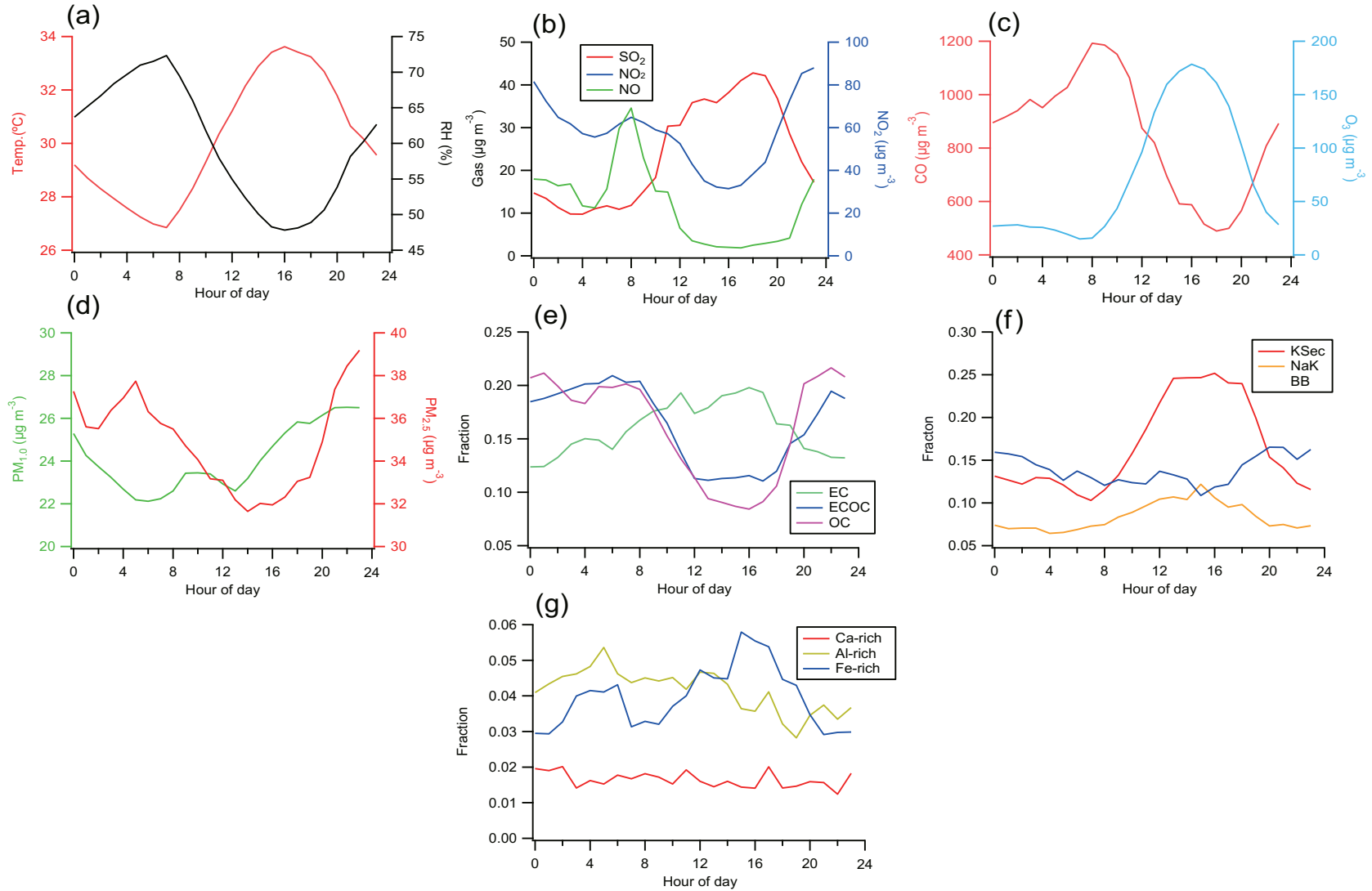


Fig. 6. Diurnal pattern of temperature, RH, gasses, and single particle types during the study.

**Table 2**

Scavenging rates of major single particle types in percentage per hour per mm precipitation. The calculation for each particle type is:  $\Delta/(\Delta \text{ precip}) = \Delta \text{ count} / (\Delta t \times \Delta \text{ precip}) \times 100$ .

Cluster	$\Delta/(\Delta \text{ precip})$ ( $\text{h}^{-1} \text{ mm}^{-1}$ ) <sup>a</sup>
NaKPb	0.61 ± 0.15
Fe-rich	0.60 ± 0.12
EC	0.58 ± 0.09
Ca-EC	0.54 ± 0.15
Ca-rich	0.51 ± 0.20
KSec	0.50 ± 0.08
OC	0.49 ± 0.16
NaK	0.43 ± 0.19
ECOC	0.36 ± 0.12
Al-rich	0.31 ± 0.22
BB	0.26 ± 0.12

<sup>a</sup> Precip stands for precipitation.

shown in Fig. 6f,  $\text{C}_2\text{H}_3\text{O}^+$  was enhanced in the range of 40–80 ppb  $\text{O}_x$ , possibly due to the water-soluble organic species uptake (Ervens et al., 2011). The enhancing of  $\text{C}_2\text{H}_3\text{O}^+$  occurred when  $\text{O}_x$  was higher than 160 ppb due to the strongly oxidative environment. Collectively, the removal of semi-volatile species in aerosol, oxidation of organic precursors in multiple pathways, and uptake of secondary species were significant in Chongqing during summertime (Ervens et al., 2011; Hallquist et al., 2009; Jimenez et al., 2009; Robinson et al., 2007).

### 3.6. Effects of RH on the evolution of single particle types

In this section, we provide insights into the effect of RH on single particle types (Fig. 9). RH influences the atmospheric behavior of aerosol in many ways. Large variations in RH during air parcel motion and temperature oscillation can affect aerosol liquid-liquid phase separation, efflorescence, and deliquescence (Zhao et al., 2006). The shift of RH can cause the change of aging processes of aerosol from gas-to-particle phase conversion to the heterogeneous or aqueous-phase pathway (McNeill, 2014). Because RH has an inverse correlation with temperature in the atmosphere (Seinfeld and Pandis, 2006), the atmospheric behavior of species affected by temperature can show a strong correlation with RH. For example, particle types containing semi-volatile organic aerosol, such as OC and ECOC, showed enrichment trends with an increase in RH (Fig. 9b) – but this effect could also arise from the decrease in temperature that caused condensation and absorption of semi-volatile species (Robinson et al., 2007). The number fraction of KSec was higher than 0.25 when RH was between 30 and 40%.

Moreover, in KSec, the abundance of  $\text{C}_2\text{H}_3\text{O}^+$  was found. This observation suggests that dry conditions favored enhancement of KS. A similar enrichment of KS was also found during winter haze days in Xi'an (Chen et al., 2016). BB decreased when RH was higher than 60%. The number fractions of EC, OC, and ECOC increased with increasing RH. These particle types, internally mixed with organic species, would be in the form of droplets when RH was low (Zhao et al., 2006). The

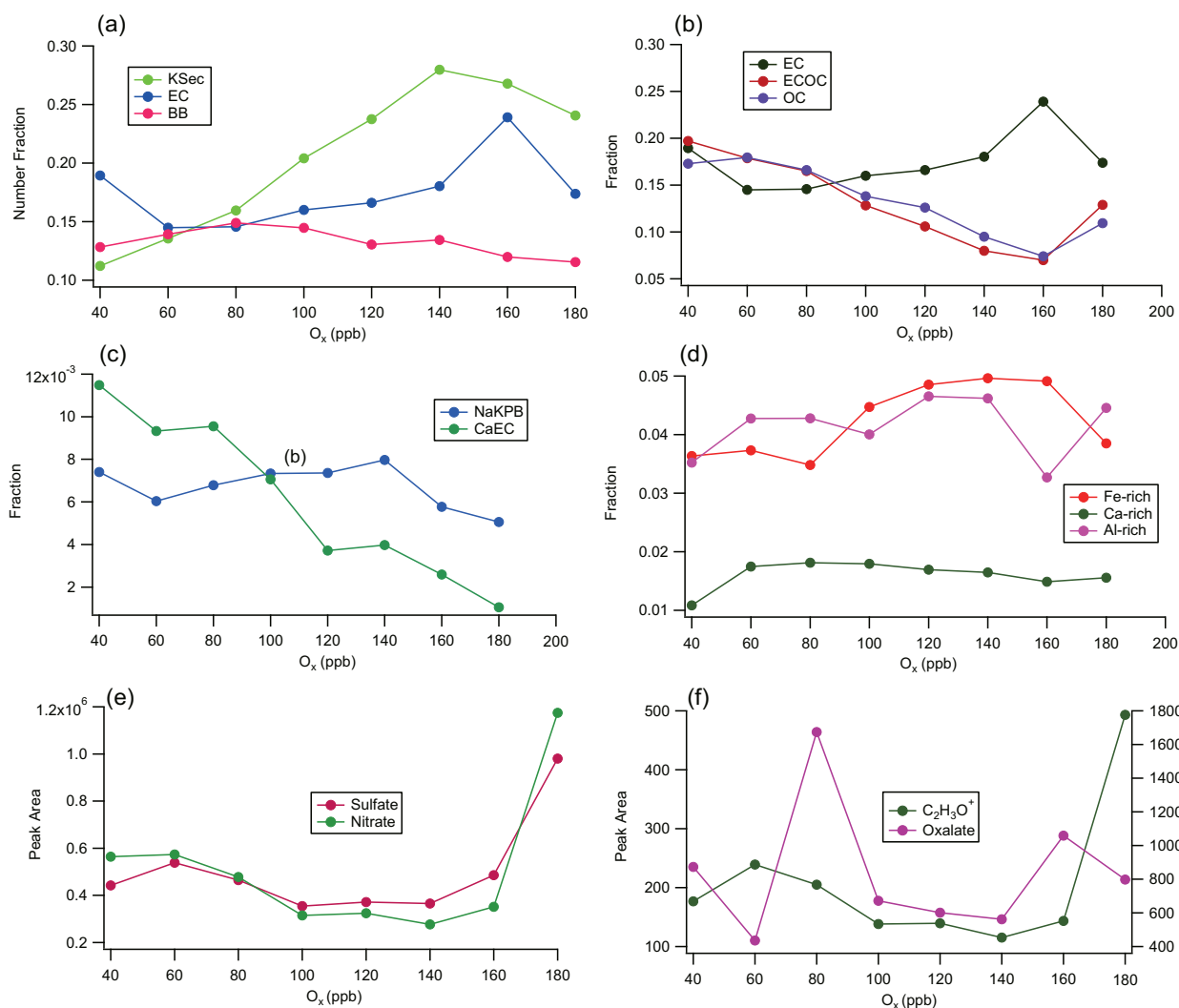


**Fig. 7.** Single particle number fractions (a, b, c, and d), and typical species such as sulfate, nitrate,  $\text{C}_2\text{H}_3\text{O}^+$ , and oxalate (e and f), versus the odd oxygen ( $\text{O}_x$ ) concentration.

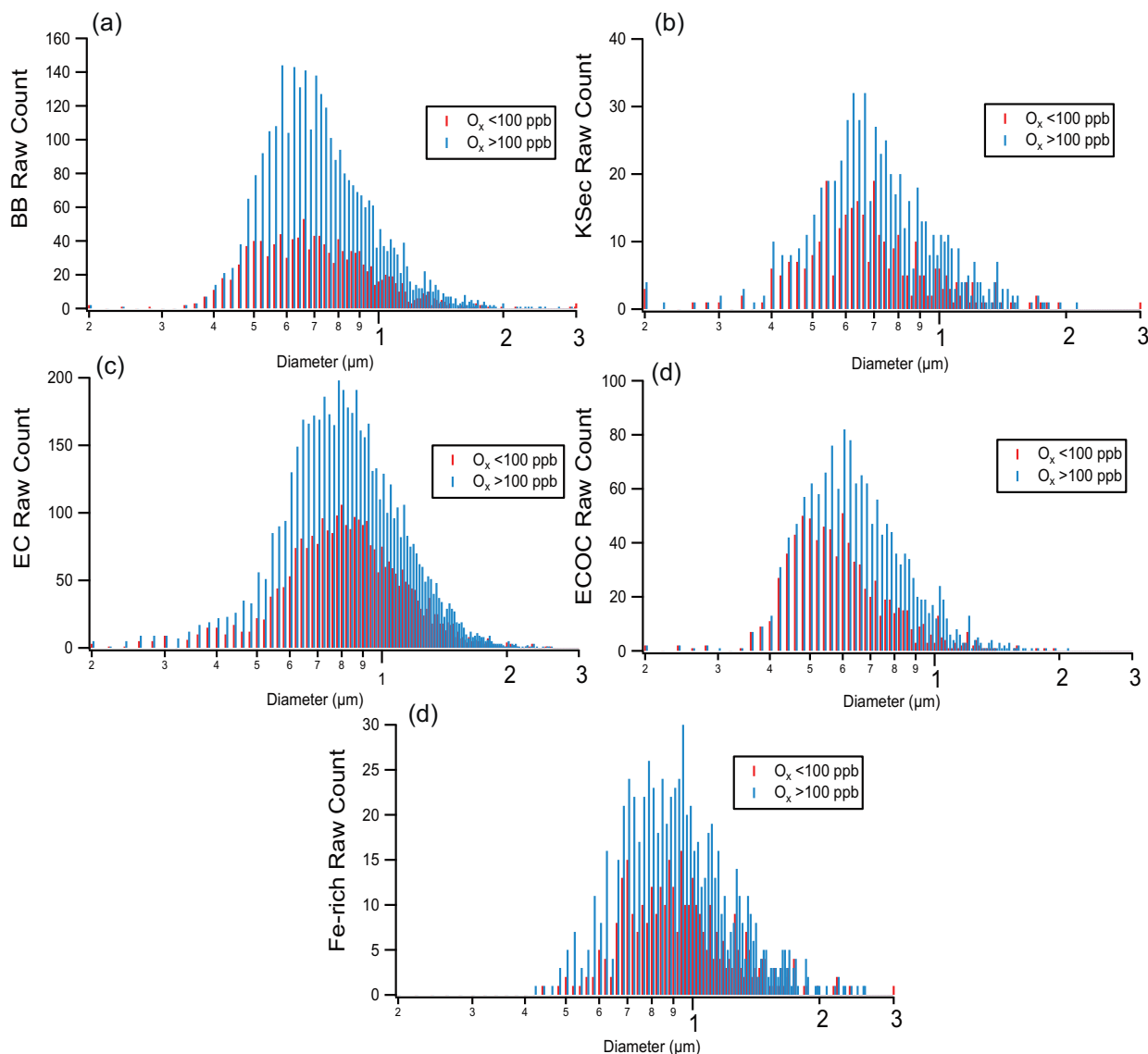


**Fig. 8.** Unscaled average size distribution of particle types when  $O_x < 100$  ppb (red stick) and  $O_x > 100$  ppb (blue stick). Y axis is the daily averaged raw count of particles.

droplets would provide a surface for multiple phase aging (McNeill, 2014). A decreasing trend of sulfate,  $C_2H_3O^+$  and nitrate peak area when RH was larger than 80% is possibly due to wet or fog scavenging of particles. However, the high RH ( $>80\%$ ) conditions favored the enrichment of oxalate.

Generally, in aging process of ambient particles, the increase of RH causes aerosol water uptake, results in the secondary aerosol formation due to aqueous and heterogeneous reactions (Ervens et al., 2011). This process is accompanied by removal of semi-volatile organic aerosol (Robinson et al., 2007), leading to shifts in the number fraction of fresh and aged particles. In an indirect way, the increasing RH enhanced OH uptake and impacts on organic aerosol lifetimes (Slade and Knopf, 2014). The aerosol lifetime variations could also result in particle type reclassification.

#### 4. Conclusions

An online measurement of urban single particle types was performed in Chongqing during summer of 2014 from 07/05 to 08/06. The major particle types were mainly carbonaceous particles and metal-rich dust. The carbonaceous particle types are mainly from

biomass/biofuel burning, traffic, and other combustion processes. The scavenging rate for single particle clusters was determined. The number fraction of particle types was strongly influenced by RH and the atmospheric oxidative level. Specifically, the number fraction of EC and KSec were enhanced with the increasing of  $O_x$  due to gas/particle phase conversion of secondary organic species. OC, EC, and ECOC were enhanced with increasing RH. This study contributes new insight into the characterization, mixing state, and evolution process of urban particles under high temperature and humid conditions in the context of Chinese air pollution.

#### Acknowledgements

The financial support from “Strategic Priority Research Program (B)” of Chinese Academy of Sciences [Grant NO. KJZD-EW-TZ-G06], National Natural Science Foundation of China [Grant NO. 41375123], “Western Talents” of Chinese Academy of Sciences, “Basic and Frontier Research Plan of Chongqing” [Grant NO. cstc2015jcyjA20003, cstc2014yykfc20003, cstckjcxljrc13], “Shanghai Science and Technology Commission, China [Grant NO. 13DZ2260900]”, and “Key Lab of Aerosol Chemistry & Physics Research Program” are acknowledged. The authors appreciate the

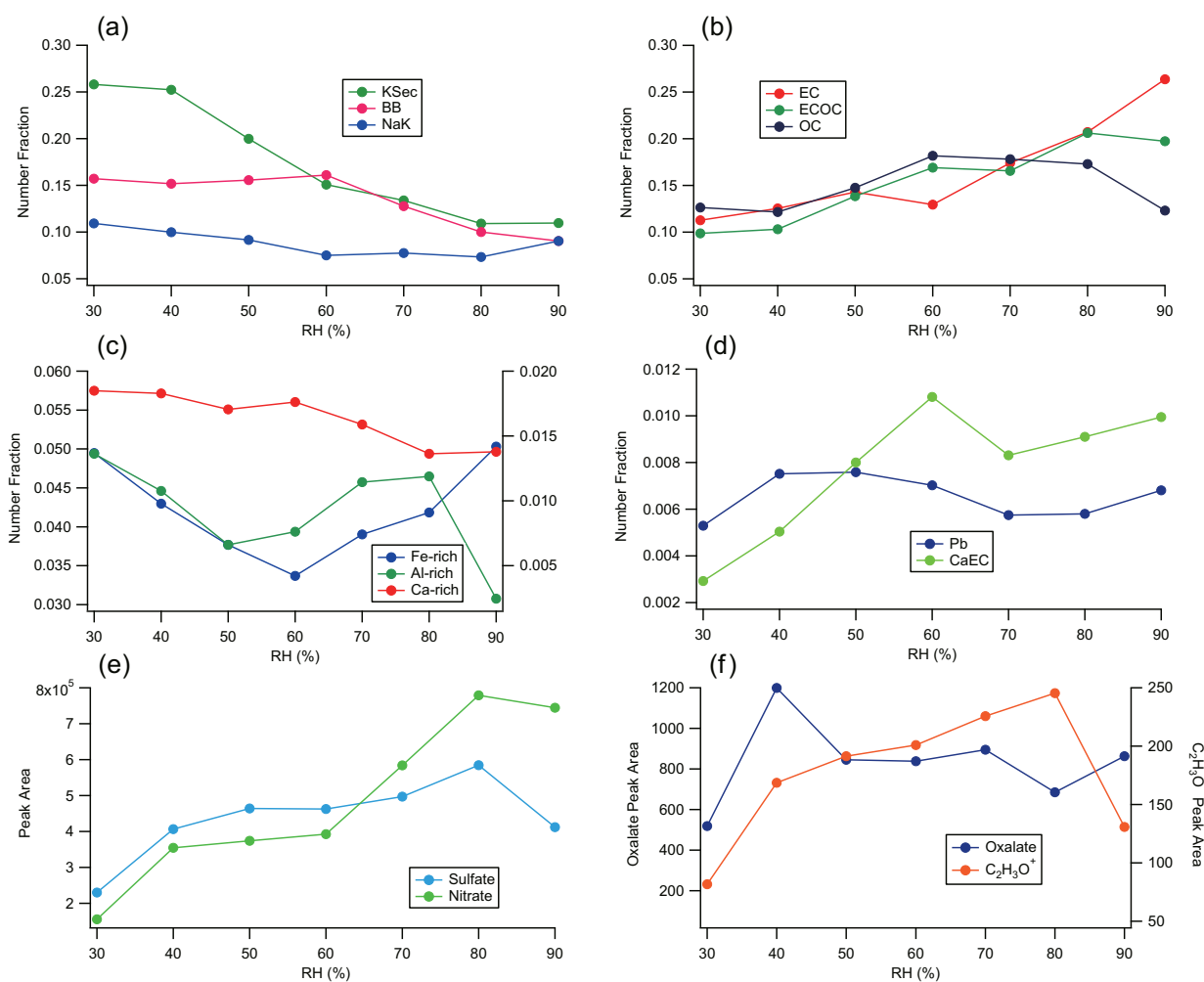


Fig. 9. Mean single particle number fractions (a, b, c, and d), and typical species such as sulfate, nitrate,  $C_2H_3O^+$ , and oxalate (e and f), versus the RH during the summer observation.

assistance from Chongqing Environmental Monitor Station for data collection and quality assurance. The authors also thank Dean Venables (University College Cork, Ireland) for editing the text.

## Appendix A. Supplementary data

Supplementary data to this article can be found online at <http://dx.doi.org/10.1016/j.atmosres.2016.12.005>.

## References

- Bi, X.H., Zhang, G.H., Li, L., Wang, X.M., Li, M., Sheng, G.Y., Fu, J.M., Zhou, Z., 2011. Mixing state of biomass burning particles by single particle aerosol mass spectrometer in the urban area of PRD, China. *Atmos. Environ.* 45, 3447–3453.
- Cao, J., 2014. *PM<sub>2.5</sub> and Environment in China*. Science Press, Beijing.
- Chen, K., Yin, Y., Kong, S., Xiao, H., Wu, Y., Chen, J., Li, A., 2014. Size-resolved chemical composition of atmospheric particles during a straw burning period at Mt. Huang (the Yellow Mountain) of China. *Atmos. Environ.* 84, 380–389.
- Chen, Y., Cao, J., Huang, R., Yang, F., Wang, Q., Wang, Y., 2016. Characterization, mixing state, and evolution of urban single particles in Xi'an (China) during wintertime haze days. *Sci. Total Environ.* 573, 937–945.
- Corbin, J.C., Rehbein, P.J.G., Evans, G.J., Abbatt, J.P.D., 2012. Combustion particles as ice nuclei in an urban environment: evidence from single-particle mass spectrometry. *Atmos. Environ.* 51, 286–292.
- Cubison, M.J., Ortega, A.M., Hayes, P.L., Farmer, D.K., Day, D., Lechner, M.J., Brune, W.H., Apel, E., Diskin, G.S., Fisher, J.A., Fuelberg, H.E., Hecobian, A., Knapp, D.J., Mikoviny, T., Riemer, D., Sachse, G.W., Sessions, W., Weber, R.J., Weinheimer, A.J., Wisthaler, A., Jimenez, J.L., 2011. Effects of aging on organic aerosol from open biomass burning smoke in aircraft and laboratory studies. *Atmos. Chem. Phys.* 11, 12049–12064.
- Dall'osto, M., Harrison, R., 2006. Chemical characterisation of single airborne particles in Athens (Greece) by ATOFMS. *Atmos. Environ.* 40, 7614–7631.
- Dall'osto, M., Harrison, R.M., 2011. Urban organic aerosols measured by single particle mass spectrometry in the megacity of London. *Atmos. Chem. Phys. Discuss.* 11, 5043–5078.
- Dall'osto, M., Beddows, D.C.S., Kinnersley, R.P., Harrison, R.M., Donovan, R.J., Heal, M.R., 2004. Characterization of individual airborne particles by using aerosol time-of-flight mass spectrometry at Mace Head, Ireland. *J. Geophys. Res. Atmos.* 109.
- Dall'osto, M., Ovadnevaite, J., Ceburnis, D., Martin, D., Healy, R.M., O'Connor, I.P., Kourtchev, I., Sodeau, J.R., Wenger, J.C., O'Dowd, C., 2013a. Characterization of urban aerosol in Cork city (Ireland) using aerosol mass spectrometry. *Atmos. Chem. Phys.* 13, 4997–5015.
- Dall'osto, M., Querol, X., Alastuey, A., O'Dowd, C., Harrison, R.M., Wenger, J., Gómez-Moreno, F.J., 2013b. On the spatial distribution and evolution of ultrafine particles in Barcelona. *Atmos. Chem. Phys.* 13, 741–759.
- Donahue, N.M., Henry, K.M., Mentel, T.F., Kiendler-Scharr, A., Spindler, C., Bohn, B., Brauers, T., Dorn, H.P., Fuchs, H., Tillmann, R., Wahner, A., Saathoff, H., Naumann, K.H., Mohler, O., Leisner, T., Müller, L., Reining, M.C., Hoffmann, T., Salo, K., Hallquist, M., Frosch, M., Bilde, M., Tritscher, T., Barmet, P., Praplan, A.P., DeCarlo, P.F., Dommen, J., Prevot, A.S., Baltensperger, U., 2012. Aging of biogenic secondary organic aerosol via gas-phase OH radical reactions. *Proc. Natl. Acad. Sci. U. S. A.* 109, 13503–13508.
- Elser, M., Huang, R.-J., Wolf, R., Slowik, J.G., Wang, Q., Canonaco, F., Li, G., Bozzetti, C., Daellenbach, K.R., Huang, Y., Zhang, R., Li, Z., Cao, J., Baltensperger, U., El-Haddad, I., Prévôt, A.S.H., 2016. New insights into PM<sub>2.5</sub> chemical composition and sources in two major cities in China during extreme haze events using aerosol mass spectrometry. *Atmos. Chem. Phys.* 16, 3207–3225.
- Ervens, B., Turpin, B.J., Weber, R.J., 2011. Secondary organic aerosol formation in cloud droplets and aqueous particles (aqSOA): a review of laboratory, field and model studies. *Atmos. Chem. Phys.* 11, 11069–11102.
- Falkovich, A.H., Graber, E.R., Schkolnik, G., Rudich, Y., Maenhaut, W., Artaxo, P., 2005. Low molecular weight organic acids in aerosol particles from Rondonia, Brazil, during the biomass-burning, transition and wet periods. *Atmos. Chem. Phys.* 5, 781–797.
- Formenti, P., Schütz, L., Balkanski, Y., Desboeufs, K., Ebert, M., Kandler, K., Petzold, A., Scheuvs, D., Weinbruch, S., Zhang, D., 2011. Recent progress in understanding physical and chemical properties of African and Asian mineral dust. *Atmos. Chem. Phys.* 11, 8231–8256.

- Gard, E., Mayer, J.E., Morrical, B.D., Dienes, T., Fergenson, D.P., Prather, K.A., 1997. Real-time analysis of individual atmospheric aerosol particles: design and performance of a portable ATOFMS. *Anal. Chem.* 69, 4083–4091.
- Gross, D.S., Galli, M.E., Silva, P.J., Prather, K.A., 2000. Relative sensitivity factors for alkali metal and ammonium cations in single-particle aerosol time-of-flight mass spectra. *Anal. Chem.* 72, 416–422.
- Hallquist, M., Wenger, J.C., Baltensperger, U., Rudich, Y., Simpson, D., Claeys, M., Dommen, J., Donahue, N.M., George, C., Goldstein, A.H., Hamilton, J.F., Herrmann, H., Hoffmann, T., Iinuma, Y., Jang, M., Jenkin, M.E., Jimenez, J.L., Kiendler-Scharr, A., Maenhaut, W., McFiggans, G., Mentel, T.F., Monod, A., Prevot, A.S.H., Seinfeld, J.H., Surratt, J.D., Szmigielski, R., Wildt, J., 2009. The formation, properties and impact of secondary organic aerosol: current and emerging issues. *Atmos. Chem. Phys.* 9, 5155–5236.
- Healy, R.M., O'Connor, I.P., Hellebust, S., Allan, A., Sodeau, J.R., Wenger, J.C., 2009. Characterisation of single particles from in-port ship emissions. *Atmos. Environ.* 43, 6408–6414.
- Healy, R.M., Hellebust, S., Kourtchev, I., Allan, A., O'Connor, I.P., Bell, J.M., Healy, D.A., Sodeau, J.R., Wenger, J.C., 2010. Source apportionment of PM<sub>2.5</sub> in Cork Harbour, Ireland using a combination of single particle mass spectrometry and quantitative semi-continuous measurements. *Atmos. Chem. Phys.* 10, 9593–9613.
- Healy, R.M., Sciare, J., Poulain, L., Kamili, K., Merkel, M., Müller, T., Wiedensohler, A., Eckhardt, S., Stohl, A., Sarda-Estève, R., McGillicuddy, E., O'Connor, I.P., Sodeau, J.R., Wenger, J.C., 2012. Sources and mixing state of size-resolved elemental carbon particles in a European megacity: Paris. *Atmos. Chem. Phys.* 12, 1681–1700.
- Healy, R.M., Evans, G.J., Murphy, M., Juranyi, Z., Tritscher, T., Laborde, M., Weingartner, E., Gysel, M., Poulain, L., Kamilli, K.A., Wiedensohler, A., O'Connor, I.P., McGillicuddy, E., Sodeau, J.R., Wenger, J.C., 2014. Predicting hygroscopic growth using single particle chemical composition estimates. *J. Geophys. Res. Atmos.* 119, 9567–9577.
- Herich, H., Kammermann, L., Friedman, B., Gross, D.S., Weingartner, E., Lohmann, U., Spichtinger, P., Gysel, M., Baltensperger, U., Cziczo, D.J., 2009. Subarctic atmospheric aerosol composition: 2. Hygroscopic growth properties. *J. Geophys. Res. Atmos.* 114.
- Huang, R.J., Zhang, Y., Bozzetti, C., Ho, K.F., Cao, J.J., Han, Y., Daellenbach, K.R., Slowik, J.G., Platt, S.M., Canonaco, F., Zotter, P., Wolf, R., Pieber, S.M., Brun, E.A., Crippa, M., Ciarelli, G., Piazzalunga, A., Schwikowski, M., Abbaszade, G., Schnelle-Kreis, J., Zimmermann, R., An, Z., Szalad, S., Baltensperger, U., El Haddad, I., Prevot, A.S., 2014. High secondary aerosol contribution to particulate pollution during haze events in China. *Nature* 514, 218–222.
- Jimenez, J.L., Canagaratna, M.R., Donahue, N.M., Prevot, A.S., Zhang, Q., Kroll, J.H., DeCarlo, P.F., Allan, J.D., Coe, H., Ng, N.L., Aiken, A.C., Docherty, K.S., Ulbrich, I.M., Grieshop, A.P., Robinson, A.L., Duplissy, J., Smith, J.D., Wilson, K.R., Lanz, V.A., Hueglin, C., Sun, Y.L., Tian, J., Laaksonen, A., Raatikainen, T., Rautiainen, J., Vaattovaara, P., Ehni, M., Kulmala, M., Tomlinson, J.M., Collins, D.R., Cubison, M.J., Dunlea, E.J., Huffman, J.A., Onasch, T.B., Alfarra, M.R., Williams, P.J., Bower, K., Kondo, Y., Schneider, J., Drewnick, F., Borrmann, S., Weimer, S., Demerjian, K., Salcedo, D., Cottrell, L., Griffin, R., Takami, A., Miyoshi, T., Hatakeyama, S., Shimojo, A., Sun, J.Y., Zhang, Y.M., Dzepina, K., Kimmel, J.R., Sueper, D., Jayne, J.T., Herndon, S.C., Trimborn, A.M., Williams, L.R., Wood, E.C., Middlebrook, A.M., Kolb, C.E., Baltensperger, U., Worsnop, D.R., 2009. Evolution of organic aerosols in the atmosphere. *Science* 326, 1525–1529.
- Kroll, J.H., Smith, J.D., Worsnop, D.R., Wilson, K.R., 2012. Characterisation of lightly oxidised organic aerosol formed from the photochemical aging of diesel exhaust particles. *Environ. Chem.* 9, 211–220.
- Li, L., Huang, Z.X., Dong, J.G., Li, M., Gao, W., Nian, H.Q., Fu, Z., Zhang, G.H., Bi, X.H., Cheng, P., Zhou, Z., 2011. Real time bipolar time-of-flight mass spectrometer for analyzing single aerosol particles. *Int. J. Mass Spectrom.* 303, 118–124.
- Li, W., Shi, Z., Zhang, D., Zhang, X., Li, P., Feng, Q., Yuan, Q., Wang, W., 2012. Haze particles over a coal-burning region in the China Loess Plateau in winter: three flight missions in December 2010. *J. Geophys. Res. Atmos.* 117 (n/a–n/a).
- Ma, L., Li, M., Huang, Z.X., Li, L., Gao, W., Nian, H.Q., Zou, L.L., Fu, Z., Gao, J., Chai, F.H., Zhou, Z., 2016. Real time analysis of lead-containing atmospheric particles in Beijing during springtime by single particle aerosol mass spectrometry. *Chemosphere* 154, 454–462.
- McNeill, V.F., 2014. *Atmospheric and Aerosol Chemistry*. Springer, Berlin Heidelberg, Berlin, Heidelberg.
- Moffet, R.C., Prather, K.A., 2009. In-situ measurements of the mixing state and optical properties of soot with implications for radiative forcing estimates. *Proc. Natl. Acad. Sci. U. S. A.* 106, 11872–11877.
- Moffet, R.C., Foy, B.D., Molina, L.A., Molina, M.J., Prather, K.A., 2008. Measurement of ambient aerosols in northern Mexico City by single particle mass spectrometry. *Atmos. Chem. Phys.* 8 (16), 4499–4516.
- Murphy, D.M., Cziczo, D.J., Froyd, K.D., Hudson, P.K., Matthew, B.M., Middlebrook, A.M., Peltier, R.E., Sullivan, A., Thomson, D.S., Weber, R.J., 2006. Single-particle mass spectrometry of tropospheric aerosol particles. *J. Geophys. Res. Atmos.* 111 (n/a–n/a).
- National-Statistics, 2014. *Chongqing Statistics 2014*. China Statistics Press, Beijing.
- Ng, N.L., Canagaratna, M.R., Jimenez, J.L., Chhabra, P.S., Seinfeld, J.H., Worsnop, D.R., 2011. Changes in organic aerosol composition with aging inferred from aerosol mass spectra. *Atmos. Chem. Phys.* 11, 6465–6474.
- Pöschl, U., 2005. Atmospheric aerosols: composition, transformation, climate and health effects. *Angew. Chem. Int. Ed. Eng.* 44, 7520–7540.
- Pratt, K.A., Prather, K.A., 2012. Mass spectrometry of atmospheric aerosols—recent developments and applications. Part II: on-line mass spectrometry techniques. *Mass Spectrom. Rev.* 31, 17–48.
- Pratt, K.A., Murphy, S.M., Subramanian, R., DeMott, P.J., Kok, G.L., Campos, T., Rogers, D.C., Prenni, A.J., Heymsfield, A.J., Seinfeld, J.H., Prather, K.A., 2011. Flight-based chemical characterization of biomass burning aerosols within two prescribed burn smoke plumes. *Atmos. Chem. Phys.* 11, 12549–12565.
- Qin, X.Y., Prather, K.A., 2006. Impact of biomass emissions on particle chemistry during the California regional particulate air quality study. *Int. J. Mass Spectrom.* 258, 142–150.
- Qin, X.Y., Pratt, K.A., Shields, L.G., Toner, S.M., Prather, K.A., 2012. Seasonal comparisons of single-particle chemical mixing state in Riverside, CA. *Atmos. Environ.* 59, 587–596.
- Robinson, A.L., Donahue, N.M., Shrivastava, M.K., Weikamp, E.A., Sage, A.M., Grieshop, A.P., Lane, T.E., Pierce, J.R., Pandis, S.N., 2007. Rethinking organic aerosols: semivolatile emissions and photochemical aging. *Science* 315, 1259–1262.
- Seinfeld, J.H., Pandis, S.N., 2006. *Atmospheric Chemistry and Physics: From Air Pollution to Climate Change*. Wiley.
- Shen, Z., Sun, J., Cao, J., Zhang, L., Zhang, Q., Lei, Y., Gao, J., Huang, R.-J., Liu, S., Huang, Y., Zhu, C., Xu, H., Zheng, C., Liu, P., Xue, Z., 2016. Chemical profiles of urban fugitive dust PM<sub>2.5</sub> samples in Northern Chinese cities. *Sci. Total Environ.* 569–570, 619–626.
- Silva, P.J., Liu, D.Y., Noble, C.A., Prather, K.A., 1999. Size and chemical characterization of individual particles resulting from biomass burning of local Southern California species. *Environ. Sci. Technol.* 33, 3068–3076.
- Silva, P.J., Carlin, R.A., Prather, K.A., 2000. Single particle analysis of suspended soil dust from Southern California. *Atmos. Environ.* 34, 1811–1820.
- Slade, J.H., Knopf, D.A., 2014. Multiphase OH oxidation kinetics of organic aerosol: the role of particle phase state and relative humidity. *Geophys. Res. Lett.* 41, 5297–5306.
- Sodeman, D.A., Toner, S.M., Prather, K.A., 2005. Determination of single particle mass spectral signatures from light-duty vehicle emissions. *Environ. Sci. Technol.* 39, 4569–4580.
- Spencer, M.T., Prather, K.A., 2006. Using ATOFMS to determine OC/EC mass fractions in particles. *Aerosol Sci. Technol.* 40, 585–594.
- Su, H., Rose, D., Cheng, Y.F., Gunthe, S.S., Massling, A., Stock, M., Wiedensohler, A., Andreae, M.O., Poschl, U., 2010. Hygroscopicity distribution concept for measurement data analysis and modeling of aerosol particle mixing state with regard to hygroscopic growth and CCN activation. *Atmos. Chem. Phys.* 10, 7489–7503.
- Sullivan, R.C., Guazzotti, S.A., Sodeman, D.A., Prather, K.A., 2007. Direct observations of the atmospheric processing of Asian mineral dust. *Atmos. Chem. Phys.* 7, 1213–1236.
- Sun, Y.L., Wang, Z.F., Fu, P.Q., Yang, T., Jiang, Q., Dong, H.B., Li, J., Jia, J.J., 2013. Aerosol composition, sources and processes during wintertime in Beijing, China. *Atmos. Chem. Phys.* 13, 4577–4592.
- Wang, G., Cheng, C., Meng, J., Huang, Y., Li, J., Ren, Y., 2015a. Field observation on secondary organic aerosols during Asian dust storm periods: formation mechanism of oxalic acid and related compounds on dust surface. *Atmos. Environ.* 113, 169–176.
- Wang, H., Zhu, B., Zhang, Z., An, J., Shen, L., 2015b. Mixing state of individual carbonaceous particles during a severe haze episode in January 2013, Nanjing, China. *Particulate* 20, 16–23.
- Xu, H., Cao, J., Ho, K., Ding, H., Han, Y., Wang, G., Chow, J., Watson, J., Khol, S., Qiang, J., 2012. Lead concentrations in fine particulate matter after the phasing out of leaded gasoline in Xi'an, China. *Atmos. Environ.* 46, 217–224.
- Yang, F., Chen, H., Wang, X., Yang, X., Du, J., Chen, J., 2009. Single particle mass spectrometry of oxalic acid in ambient aerosols in Shanghai: mixing state and formation mechanism. *Atmos. Environ.* 43, 3876–3882.
- Yang, F., Wang, X., Zhang, Y., Wang, X., Chen, H., Yang, X., Chen, J., 2010. Real-time, single-particle measurements of ambient aerosols in Shanghai. *Front. Chem. China* 5, 331–341.
- Yang, F., Chen, H., Du, J.F., Yang, X., Gao, S., Chen, J.M., Geng, F.H., 2012. Evolution of the mixing state of fine aerosols during haze events in Shanghai. *Atmos. Res.* 104, 193–201.
- Ye, D., Zhao, Q., Jiang, C.T., Chen, J., Meng, X.X., 2007. Characteristics of elemental carbon and organic carbon in PM<sub>10</sub> during spring and autumn in Chongqing, China. *China Part. 5*, 255–260.
- Ye, Q., Robinson, E.S., Ding, X., Ye, P., Sullivan, R.C., Donahue, N.M., 2016. Mixing of secondary organic aerosols versus relative humidity. *Proc. Natl. Acad. Sci.*
- Zamora, L.M., Prospero, J.M., Hansell, D.A., Trapp, J.M., 2013. Atmospheric P deposition to the subtropical North Atlantic: sources, properties, and relationship to N deposition. *J. Geophys. Res. Atmos.* 118, 1546–1562.
- Zauscher, M.D., Wang, Y., Moore, M.J., Gaston, C.J., Prather, K.A., 2013. Air quality impact and physicochemical aging of biomass burning aerosols during the 2007 San Diego wildfires. *Environ. Sci. Technol.* 47, 7633–7643.
- Zhai, J.H., Wang, X.N., Li, J.Y., Xu, T.T., Chen, H., Yang, X., Chen, J.M., 2015. Thermal desorption single particle mass spectrometry of ambient aerosol in Shanghai. *Atmos. Environ.* 123, 407–414.
- Zhang, Q., Jimenez, J.L., Canagaratna, M.R., Ulbrich, I.M., Ng, N.L., Worsnop, D.R., Sun, Y., 2011. Understanding atmospheric organic aerosols via factor analysis of aerosol mass spectrometry: a review. *Anal. Bioanal. Chem.* 401, 3045–3067.
- Zhao, P., Feng, Y., Zhu, T., Wu, J., 2006. Characterizations of resuspended dust in six cities of North China. *Atmos. Environ.* 40, 5807–5814.